CHAPTER 6

COMPARATIVE STUDIES OF INLINE AND STAGGERED TUBE BUNDLES BASED ON TES SYSTEM INTEGRATED WITH ENGINE EXHAUST FOR CABIN HEATING

This chapter is broadly divided into three sections in which the theoretical and experimental study with inline & staggered tube bundles-based TES system integrated with engine exhaust. In the first section, the theoretical performance analysis for the inline and staggered tube bundle-based heat exchangers has been discussed and compared based on the various correlations. These heat exchangers were integrated with the engine exhaust, and the performance analysis was evaluated with the help of selected organic PCM/NEPCMs, in the second section. In the third section, the designed TES systems using Lauric acid with 0.1% vol. fraction Al_2O_3, paraffin wax with 0.02% vol. fraction MWCNT and stearic acid with 0.1% vol. fraction of CuO-based organic PCM/NEPCMs were used for the cabin heating purpose, and thermal performance analysis has been discussed.

6.1. Theoretical study on inline and staggered types tube bundles based on TES system

In this section, a theoretical study of multitube types-based TES systems has been done. Inline and staggered types of tube bundles based on the TES system have been

considered in the study. The results were found with Grimsom & E.D, Kays et al., and Zukauskas & A. Correlations. TES system with model description and governing equation for calculation of parameters have been discussed in the following subsections.

6.1.1. Design description of TES system and governing equations

In the proposed study, a comparison has been made of tube bundles-based TES systems filled with PCM/NEPCMs. The TES systems are charged with heat transfer fluid (water). The term charging means the HTF temperature equals the PCM temperature filled in TES systems. In the study, the charging temperature was considered 80^{o}C, and the numbers of 5 concentric tube-type TES systems were taken. The tubes were arranged in an inline and staggered tubes arrangement. The normal and parallel spacing of two consecutive tubes is 1.25 multiplied by the tube diameter. Effect of outlet air temperature, the pressure drop across tubes, Nusselts and Reynolds numbers, convective heat transfer coefficient, and heat transfer rate on outer tube diameter range of 0.02-0.2m, air velocity range of 1-10 m/s, and a tube length range of 0.1-1m. The tube arrangements for inline and staggered based heat exchangers have been presented in Figs. 6.1(a-b). Also, Table 6.1 represents the geometrical modeling of the TES system.

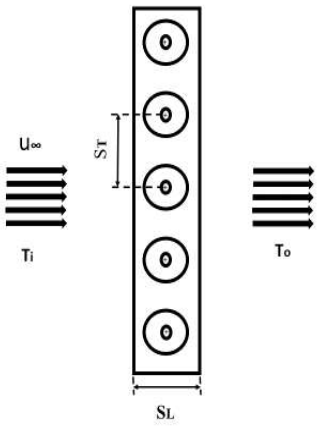

Fig.6.1(a). Inline tube arrangement

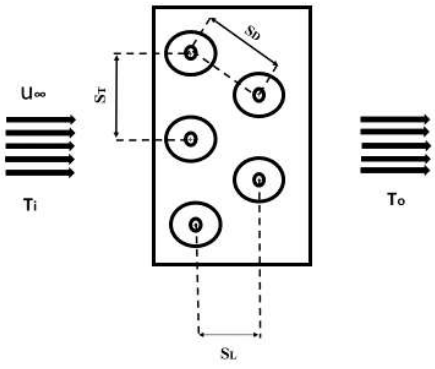

Fig.6.1(b). Staggered tube arrangement

Table 6.1: The geometrical description of the TES system

Parameters	Inline tube type TES system	Staggered tube type TES system
Outer tube diameters(mm)	Variation from 0.02 to 0.2m	Variation from 0.02 to 0.2m
Length of tube	Variation from 0.1 to 1m	Variation from 0.1 to 1m
Number of inner tubes	5	5
Number of inner tubes	5	5
Material of tube	Stainless steel(304) (Cr-18%,Ni-8%,C-0.08%)	Stainless steel(304) (Cr-18%,Ni-8%,C-0.08%)
Air velocity	Variation from 1m/s to 10m/s	Variation from 1m/s to 10m/s

Based on the literature survey such as (Grimson, 1937) (Kays et al., 1952) and (Zukauskas, 1987) following governing equations have been found:

The maximum flow velocity (u_{max}) can be represented as:

$$u_{max} = u_{\infty}\left[\frac{Sn}{S_n - D}\right] \text{ (valid for inline tubes arrangement)} \quad (6.1a)$$

$$u_{max} = u_{\infty}\left[\frac{\frac{Sn}{2}}{\left[\left(\frac{S_n}{2}\right)^2 + S_p^2\right]^{0.5} - D}\right] \text{(valid for staggered tubes arrangement)} \quad (6.1b)$$

Reynolds number (Re_{max}) for the fluid within the tubes can be represented as:

$$\mathrm{Re}_{max} = \frac{u_{\times max} \times D \times \rho}{\mu} \quad (6.2)$$

Prandtl number (Pr) for the fluid within the tubes can be expressed as:

$$\mathrm{Pr} = \frac{\mu \times c_p}{k} \quad (6.3)$$

Pressure drop for the flow of gases over a bank of tubes (δp): can be expressed as:

$$\delta p = \frac{2 \times f \times G_{max}^2 \times N}{\rho} \left(\frac{\mu_w}{\mu_b}\right)^{0.14} \text{(Grimson, 1937)} \quad (6.4a)$$

$$\text{where } f = \left\{0.25 + \frac{0.118}{\left[\frac{S_n - D}{D}\right]^{1.08}}\right\} Re_{max}^{-0.16} \text{ (valid for staggered tube arrangement)} \quad (6.4b)$$

$$f = \left\{0.044 + \frac{0.08 \times \frac{S_p}{D}}{\left[\frac{S_n - D}{D}\right]^{0.43 + 1.13 \times \frac{S_p}{D}}}\right\} Re_{max}^{-0.15} \text{(valid for inline tube arrangement)}$$

$$\delta p = \frac{Eu}{X} \times X \times \frac{1}{2} \times u_{max}^2 \times \rho \times N \text{(Zukauskas, 1987))} \quad (6.4c)$$

Nusselt number (Nu) valid for inline and staggered tube arrangements: (Grimson, 1937)

$$\mathrm{Nu} = C \times Re_{max}^n \times Pr^{0.36} \times \left(\frac{Pr}{Pr_w}\right)^{0.25} \quad (6.5a)$$

Again, the Nusselt number is valid for inline tube arrangements: (Zukauskas, 1987)

$$\mathrm{Nu} = 0.9 \times c_n \times Re_{max}^{0.4} \times Pr^{0.36} \times \left(\frac{Pr}{Pr_w}\right)^{0.25} \quad (\text{valid for } \mathrm{Re}_{max} = 1\text{-}10^2) \quad (6.5b)$$

$$\mathrm{Nu} = 0.52 \times c_n \times Re_{max}^{0.5} \times Pr^{0.36} \times \left(\frac{Pr}{Pr_w}\right)^{0.25} \quad (\text{valid for } \mathrm{Re}_{max} = 10^2\text{-}10^3) \quad (6.5c)$$

$$Nu=0.27\times c_n \times Re_{max}^{0.63} \times Pr^{0.36} \times \left(\frac{Pr}{Pr_w}\right)^{0.25} \quad \text{(valid for } Re_{max}=10^3\text{-}2\times10^5\text{)} \tag{6.5d}$$

$$Nu=0.033\times c_n \times Re_{max}^{0.8} \times Pr^{0.36} \times \left(\frac{Pr}{Pr_w}\right)^{0.25} \quad \text{(valid for } Re_{max}=2\times10^5\text{-}2\times10^6\text{)} \tag{6.5e}$$

Also, the Nusselt number is valid for staggered tube arrangement: (Zukauskas, 1987)

$$Nu=1.04\times c_n \times Re_{max}^{0.4} \times Pr^{0.36} \times \left(\frac{Pr}{Pr_w}\right)^{0.25} \text{(valid for } Re_{max}=1\text{-}500\text{)} \tag{6.5f}$$

$$Nu=0.71\times c_n \times Re_{max}^{0.5} \times Pr^{0.36} \times \left(\frac{Pr}{Pr_w}\right)^{0.25} \text{(valid for } Re_{max}=500\text{-}10^3\text{)} \tag{6.5g}$$

$$Nu=0.35\times c_n \times Re_{max}^{0.6} \times Pr^{0.36} \times \left(\frac{Pr}{Pr_w}\right)^{0.25} \times \left(\frac{S_t}{S_l}\right)^{0.2} \text{(valid for } Re_{max}=10^3\text{-}2\times10^5\text{)} \tag{6.5h}$$

$$Nu=0.031\times c_n \times Re_{max}^{0.8} \times Pr^{0.36} \left(\frac{Pr}{Pr_w}\right)^{0.25} \times \left(\frac{S_t}{S_l}\right)^{0.2} \text{(valid for } Re_{max}=2\times10^5\text{-}2\times10^6\text{)} \tag{6.5i}$$

Where $c_n = 0.95$ (6.5j)

$$Nu = \frac{h\times l}{k}$$

However, the heat transfer rate (Q), which is valid for inline and staggered tube arrangements: (Grimson, 1937) and (Zukauskas, 1987)

$$Q = h\times A\times\left[Tw - \left(\frac{T_i - T_o}{2}\right)\right] \tag{6.6a}$$

According to (Kays et al., 1952) a correlation that is valid for inline and staggered tube arrangement is the heat transfer rate;

$$Q = h_c \times A \times \left[Tw - \left(\frac{T_i - T_o}{2} \right) \right] \quad (6.6b)$$

Where $h_c = r \times h$

Also, according to (Grimson, 1937), (Kays et al., 1952), and (Zukauskas, 1987), which is valid for inline and staggered tube arrangements,

$$Q = m_a \times c_p \times [T_o - T_i] \quad (6.6c)$$

6.1.2. Results and discussion

In this section, outlet temperature, pressure drop, Nusselt number, Raynold's number, heat transfer coefficient, and heat transfer rate on tube diameter, air velocity, and tube length have been discussed and compared inline and staggered tube arrangements.

6.1.2.1. Variation in air outlet temperature with tube diameter, air velocity, and tube length

The air outlet temperature variation with tube diameter at constant air velocity and tube length for inline and staggered tube arrangement has been presented in Figs. 6.2(a-b). An increment in tube diameter, perform the decrease in air outlet temperature in inline and staggered tube arrangements. The air outlet temperature was reduced by 0.39%, with the tube diameter increasing from 0.02m to 0.2m, according to the correlation given by Zukauskas and A.A. for both tube arrangements, respectively. The optimum air outlet temperature was obtained in both tube arrangement cases at 0.02m tube diameter. However, the air temperature variation at the outlet with air velocity at constant tube diameter and tube length for inline and staggered tube arrangement, respectively, has been shown as Figs. 6.3(a-b). With variation in air velocity from 1 to 10m/s, the air outlet temperature decreased at both tube arrangement and the maximum value obtained at

minimum air velocity. Accordingly to Zukauskas and A.A. correlation, the air outlet temperature decreased by 0.46% and 0.23%, incrementing air velocity from 1m/s to 10m/s for inline and staggered tube arrangements, respectively.

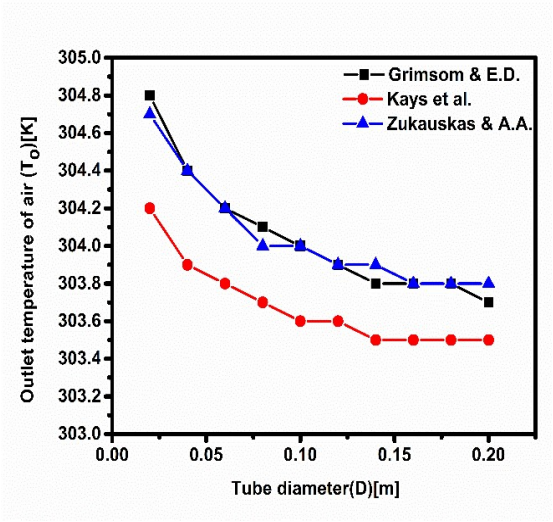

Fig.6.2(a). Variation in air outlet temperature with tube diameter(D) at u=2m/s and l=0.3m (inline tube arrangement)

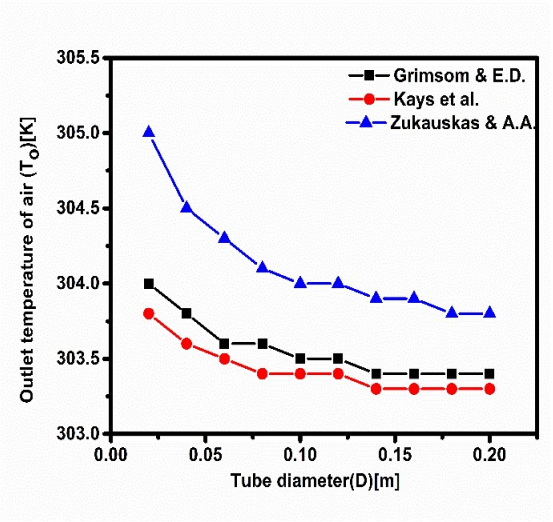

Fig.6.2(b). Variation in air outlet temperature with tube(D) diameter at u=2m/s & l=0.3m (staggered tube arrangement)

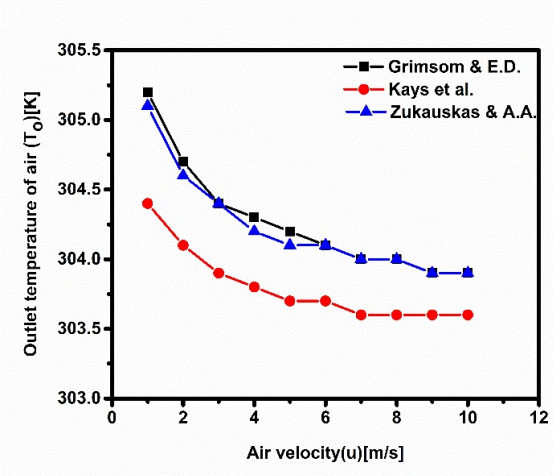

Fig.6.3(a). Variation in air outlet temperature with air velocity(u) at D=0.0254m and l=0.3m (inline tube arrangement)

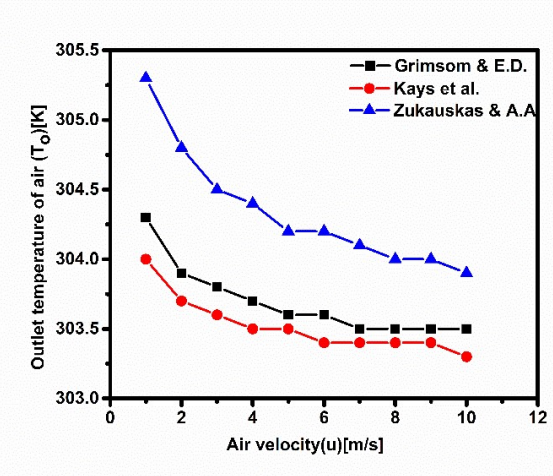

Fig.6.3(b). Variation in air outlet temperature with air velocity(u) at D=0.0254m & l=0.3m (staggered tube arrangement)

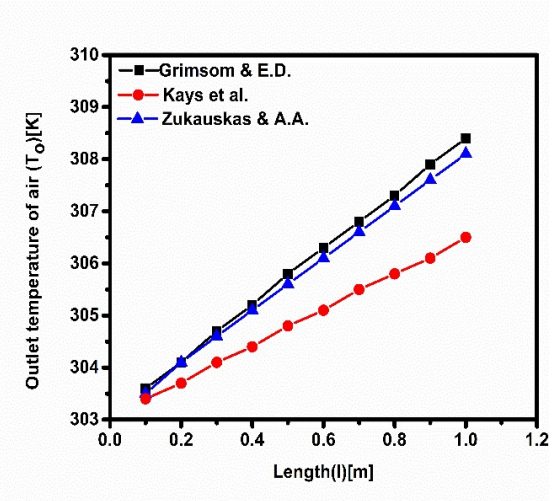

Fig.6.4(a). Variation in air outlet temperature with length of tube(l) at D=0.0254m & u=2m/s (inline tube arrangement)

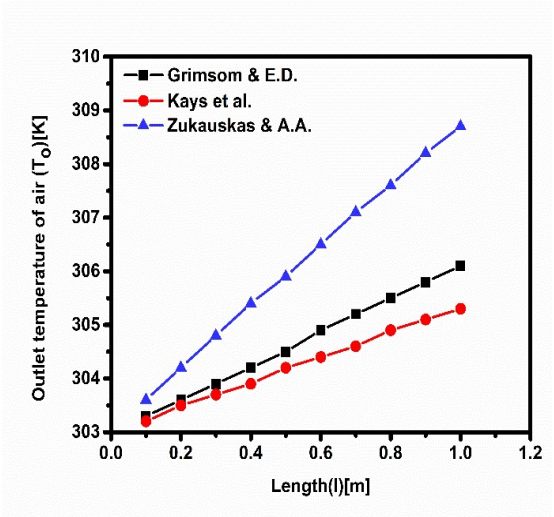

Fig.6.4(b). Variation in air outlet temperature with length of tube(l) at D=0.0254m & u=2m/s (staggered tube arrangement)

Figs. 6.4(a-b) revealed the variation of air outlet temperature with the length of tubes at constant tube diameter and air velocity for inline and staggered tube arrangement, respectively. However, the air outlet temperature increased by 1.52% and 1.68%, with an increment in tube length from 0.1m to 1m for inline and staggered tube arrangement, respectively, according to Zukauskas and A. A correlation,

6.1.2.2. Variation in pressure drop with tube diameter and air velocity

The pressure drop variation with tube diameter at constant air velocity and tube length in inline and staggered tube arrangement, respectively, has been presented in Figs. 6.5(a-b). The result shows that in the inline tube arrangement, the pressure drop decreased with an increment in tube diameter from 0.02m to 0.2m. However, the pressure drop increased with tube diameter in the staggered tube arrangement. Also, the pressure drop across the tubes was almost constant with tube diameter for staggered tube arrangement,

according to Grimson and E.D. correlation. But, the pressure drop across the tubes decreased by 93.2 pascals for inline tube arrangement in the case of Zukauskas and A.A. Correlations.

Furthermore, in the staggered tube arrangement, the pressure drop across the tubes increased by 116.5 pascals with a tube diameter from 0.02m to 0.2m. As the diameter increases, the Reynolds number of the heat transfer fluid also increases. From the pressure drop expression, the pressure drop depends on the friction factor, and the friction factor is reduced by increasing the Reynolds number. In the case of staggered tube arrangement, the number of tube rows increases, and hence, pressure drop increases with tube diameter.

The variation in pressure drop across the tubes with air velocity for constant tube diameter and tube length in inline and staggered tube arrangements are shown in Figs. 6.6(a-b). According to Grimson and E.D. correlation, the pressure drop across the tubes increased by 2179.77 pascals and 5825.87 pascals with air velocity variation from 1 m/s to 10 m/s for inline and staggered tube arrangement, respectively. From Bernoulli's equation, kinetic energy increases with an increment in airflow velocity, and hence pressure drop rises rapidly.

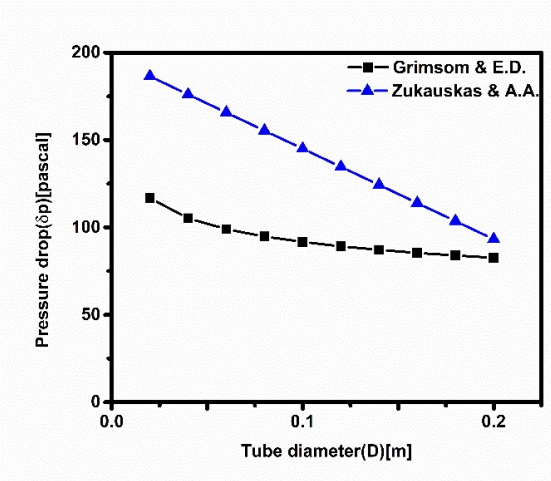

Fig.6.5(a). Variation in pressure drop (δp) with tube(D) diameter at u=2m/s & l=0.3m (inline tube arrangement)

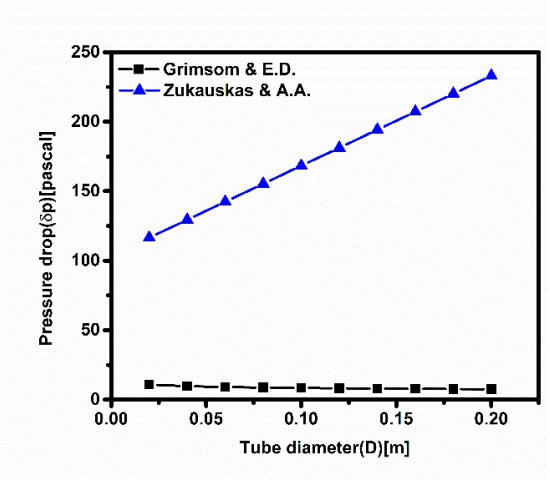

Fig.6.5(b). Variation in pressure drop (δp) with tube(D) diameter at u=2m/s & l=0.3m (staggered tube arrangement)

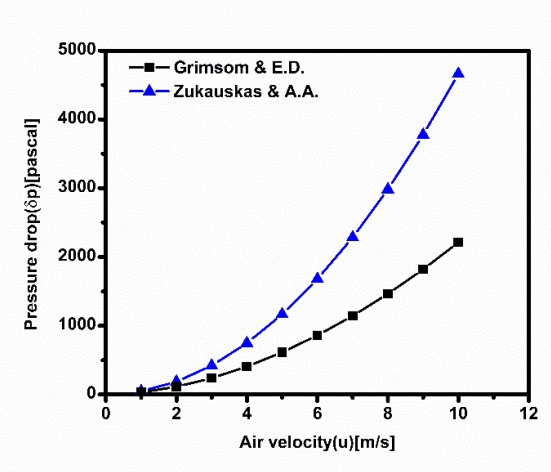

Fig.6.6(a). Variation in pressure drop (δp) with air velocity(u) at D=0.0254m & l=0.3m (inline tube arrangement)

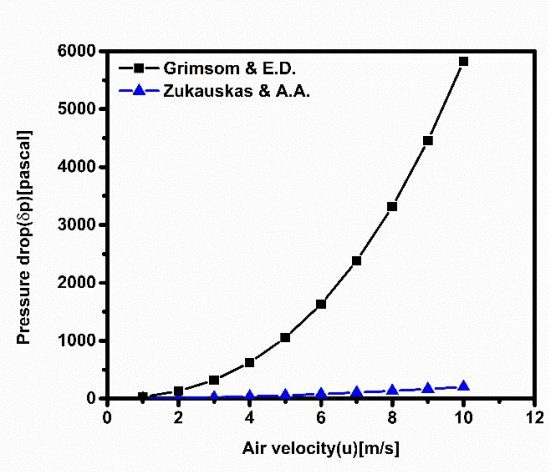

Fig.6.6(b). Variation in pressure drop (δp) with air velocity(u) at D=0.0254m & l=0.3m (staggered tube arrangement)

6.1.2.3. Variation in Nusselt and Reynolds number with tube diameter and air velocity

According to Zukauskas and A. A correlation, Figs. 6.7(a-b), showed the Nusselt and Reynolds number variation with tube diameter at constant air velocity and tube length for inline and staggered tube arrangements. In the inline and staggered tube arrangements, the Nusselt number increased by 326.6% and 298%, respectively, for an increment in tube diameter from 0.02m to 0.2m. Also, the Reynolds number increased by 900% with an increment in tube diameter from 0.02m to 0.2m in both the tube arrangements. However, the Nusselt and Reynolds number variation with air velocity at constant tube diameter and tube length for inline and staggered tube arrangement, shown in Figs. 6.8(a-b) according to Zukauskas and A. A correlation. Results revealed that with an increase in the air velocity from 1m/s to 10m/s, the Nusselt number increased by 326.6% and 298% in the case of inline and staggered tube arrangements, respectively. However, in the case of inline and staggered tube arrangement, the Reynolds number increased by 900%, increasing air velocity from 1m/s to 10m/s.

Furthermore, the Reynolds number depends on the maximum average air velocity, outer tube diameter, and other air thermophysical (density and viscosity). With an increment in tube diameter and air velocity, the Reynolds number also increases. The Nusselt number is a function of geometry parameters, Reynolds number, and Prantl number at the wall and bulk mean temperature. Due to constant geometry parameters and thermophysical properties, the Nusselt number will increase with an increment in the Reynolds number.

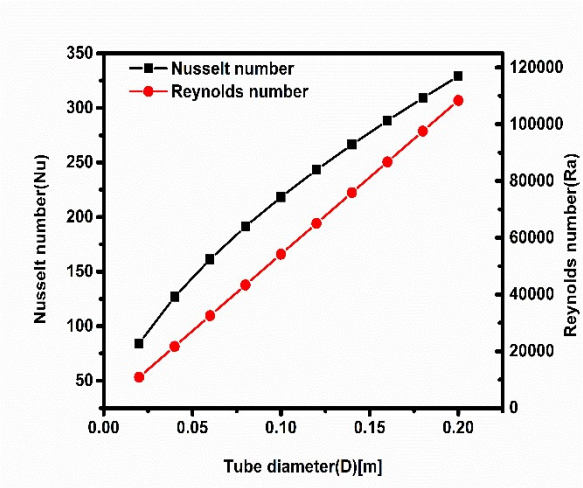

Fig.6.7(a). Variation in Nusselt and Reynolds number with tube(D) diameter at u=2m/s & l=0.3m (inline tube arrangement)

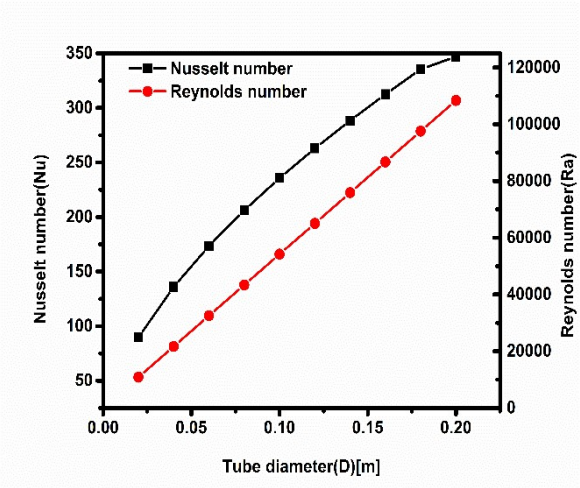

Fig.6.7(b). Variation in Nusselt and Reynolds number with tube(D) diameter at u=2m/s & l=0.3m (staggered tube arrangement)

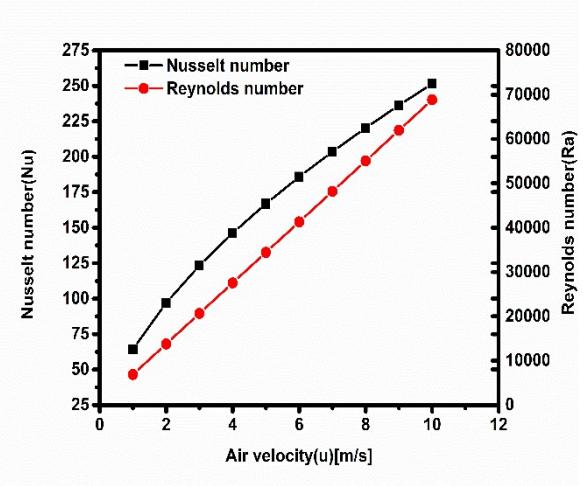

Fig.6.8(a). Variation in Nusselt and Reynolds number with air velocity(u) at D=0.0254m & l=0.3m (inline tube arrangement)

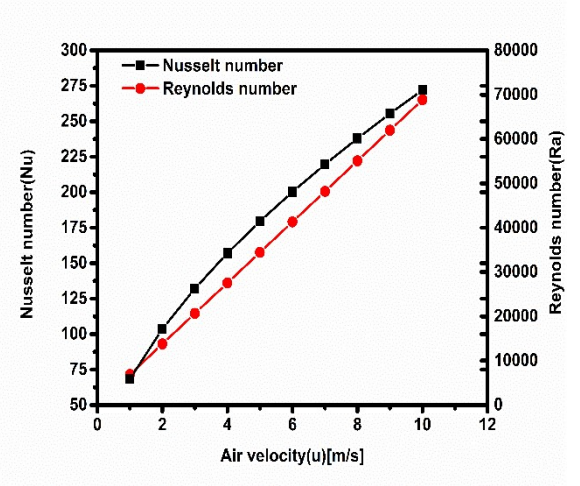

Fig.6.8(b). Variation in Nusselt and Reynolds number with air velocity(u) at D=0.0254m & l=0.3m (staggered tube arrangement)

6.1.2.4. Variation in convective heat transfer coefficient with tube diameter and air velocity

Furthermore, Figs. 6.9(a-b) shows the convective heat transfer coefficient variation with tube diameter at constant air velocity and tube length for inline and staggered tube arrangements. Results revealed that the convective heat transfer decreased with an increment of the tube diameter. The convective heat transfer decreased by 57.3% and 60% for an increment in tube diameter from 0.02m to 0.2m for inline and staggered tube arrangements, respectively, according to Zukauskas and A. A correlation. Due to an increment in the tube diameter, the heat exchange area increases, and the outlet air temperature decreases, decreasing the convective heat transfer coefficient. Also, the convective heat transfer coefficient increased by 326% and 298% with an increment in air velocity from 1m/s to 10m/s for constant tube diameter and tube length for both the tube arrangements, as shown in Figs. 6.10(a-b), according to Zukauskas and A. A correlation. With an increase in air velocity, the pressure drops, and the Reynolds number increases, which influences the heat transfer coefficient.

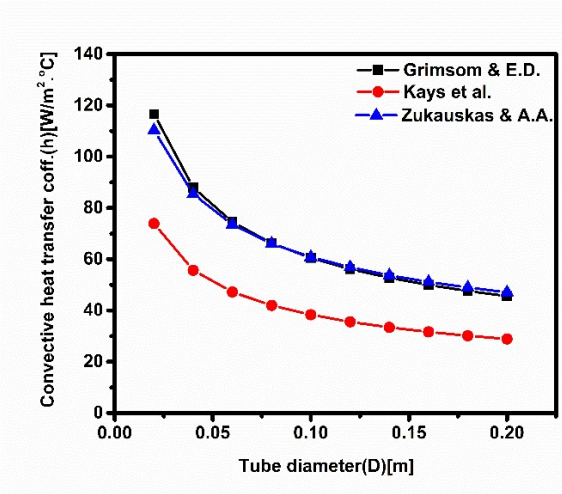

Fig.6.9(a). Variation in convective heat transfer coefficient with tube diameter(D) at u=2m/s and l=0.3m (inline tube arrangement)

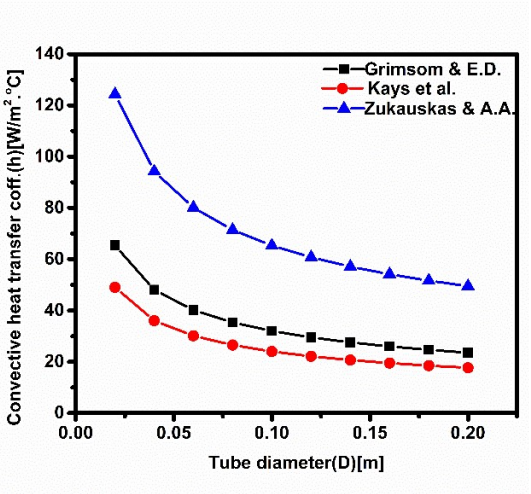

Fig.6.9(b). Variation in convective heat transfer coefficient with tube diameter(D) at u=2m/s and l=0.3m (staggered tube arrangement)

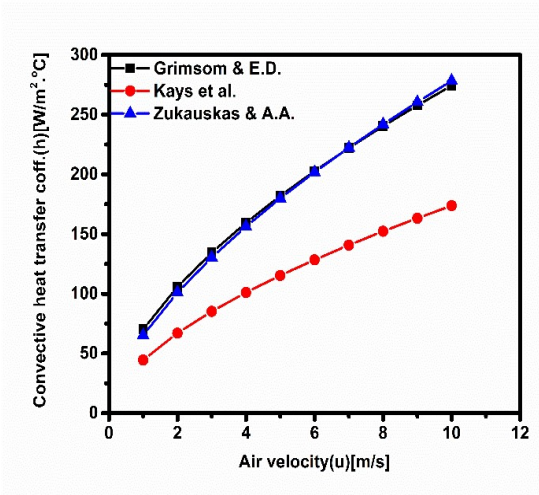

Fig.6.10(a). Variation in convective heat transfer coefficient with air velocity(u) at D=0.0254m and l=0.3m (inline tube arrangement)

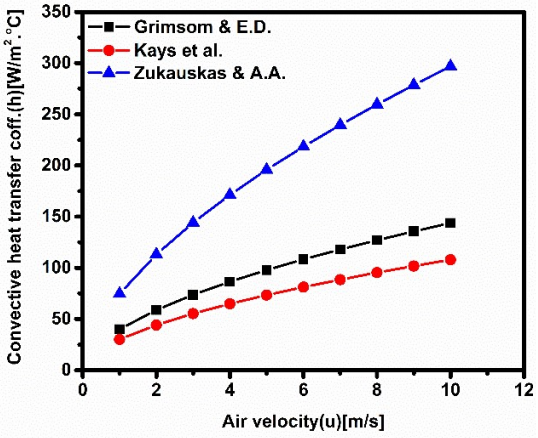

Fig.6.10(b). Variation in convective heat transfer coefficient with air velocity(u) at D=0.0254m and l=0.3m (staggered tube arrangement)

6.1.2.5. Variation in energy transfer rate with tube diameter, air velocity, and tube length

Figs. 6.11(a-b) represent the energy transfer rate which increases with an increment in the tube diameter at constant air velocity and tube length. Results revealed that the energy transfer rate improved by 330.8% and 302.9% for an increment in tube diameter from 0.02m to 0.2m for inline and staggered tube arrangements, respectively, according to Zukauskas and A. A correlation, as the air velocity increases from 1m/s to 10m/s, the energy transfer rate also improved by 331.5% and 303.7% for inline and staggered tube arrangements, respectively, as shown in Figs. 6.12(a-b). The energy transfer rate increased by 853.8% and 848.6%, with the tube length variation from 0.1m to 1m for both the tube arrangement cases, according to Zukauskas and A. A correlation, as shown in Figs. 6.13(a-b). The maximum variation in the energy transfer rate is shown in Zukauskas and A. A correlation than other considered correlations for inline and staggered tube arrangements. Furthermore, an increment in tube diameter, air velocity, tube length, the heat exchange surface area, and temperature difference also increased, improving the heat transfer rate.

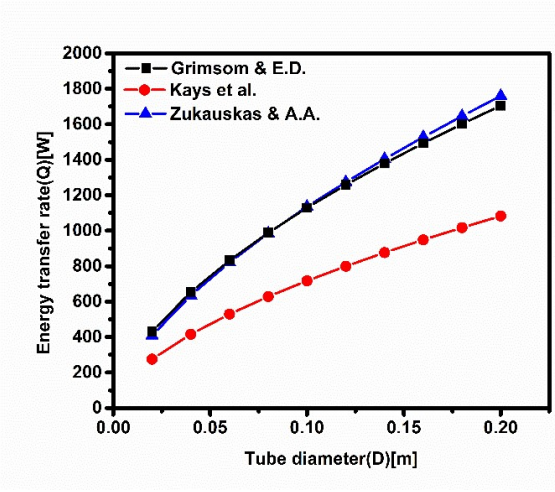

Fig.6.11(a). Variation in energy transfer rate with tube diameter(D) at u=2m/s and l=0.3m (inline tube arrangement)

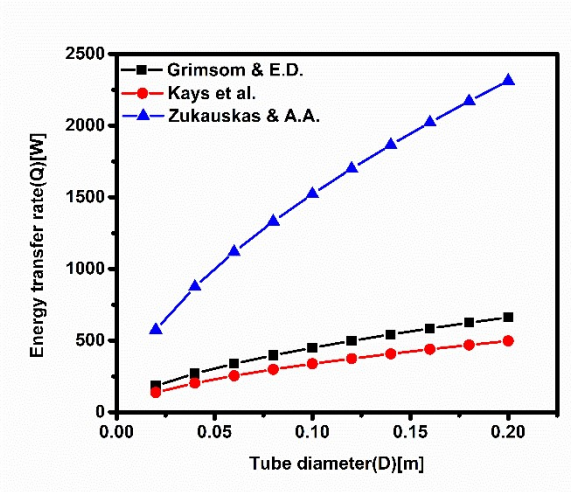

Fig.6.11(b). Variation in energy transfer rate with tube(D) diameter at u=2m/s & l=0.3m (staggered tube arrangement)

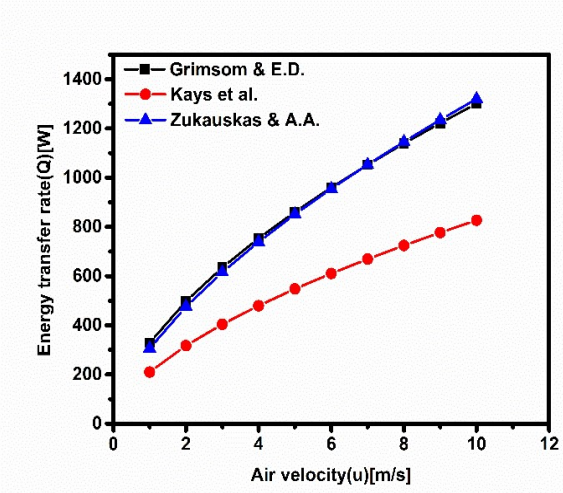

Fig.6.12(a). Variation in energy transfer rate with air velocity(u) at D=0.0254 m and l=0.3 m (inline tube arrangement)

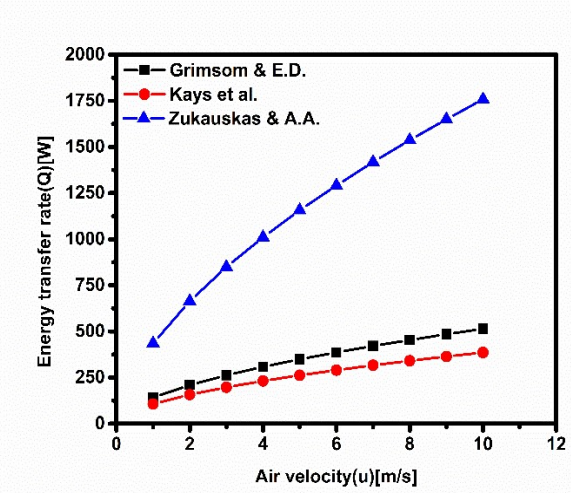

Fig.6.12(b). Variation in energy transfer rate with air velocity(u) at D=0.0254 m & l=0.3 m (staggered tube arrangement)

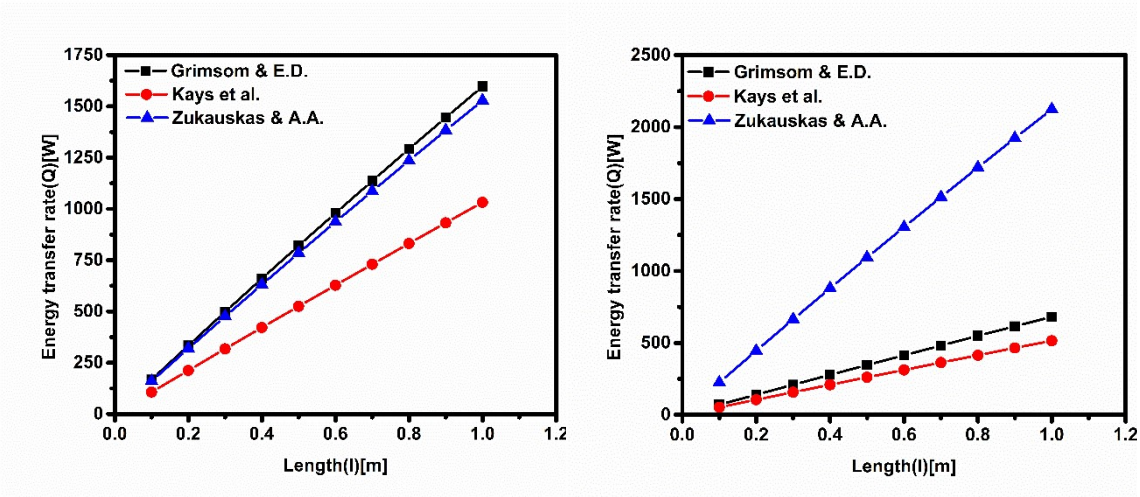

Fig.6.13(a). Variation in energy transfer rate with length of tube(l) at D=0.0254m & u=2m/s (inline tube arrangement)

Fig.6.13(b). Variation in energy transfer rate with length of tube(l) at D=0.0254m & u=2m/s (staggered tube arrangement)

In the inline tube arrangement case, the variation profile of air temperature at the outlet, convective heat transfer coefficient, and the energy transfer rate with tube diameter, air velocity, and tube length revealed almost similar to Grimson and E. D. correlation and Zukauskas and A. A correlation case. But in the case of staggered tube arrangement, the variation profile of air temperature at the outlet, convective heat transfer coefficient, and energy transfer rate have similar trends for Grimson and E.D. correlation and Kays et al. correlation case.

6.2. Thermal performance of inline and staggered tube bundles type TES system integrated with IC engine.

In this section, the effect of thermal performance for inline and staggered tube bundles type TES system integrated with IC engine have been discussed and compared.

6.2.1. Detail of experiment setup and procedure:

The experiment was conducted on the same test rig as discussed in chapter 3. Figs. 6.14(a-b) shows the diagram of the experimental setup. Instead of the concentric tube type TES system, the inline and staggered tube bundles type TES system was used. The diagram and the specification of tube bundles type TES system were shown in Figs. 6.15(a-b) and Table .6.2, respectively. The TES system was filled with lauric acid with vol. fraction 0.1% Al_2O_3, paraffin wax with 0.02% MWCNT and stearic acid with 0.1% CuO NEPCMs. The samples of PCMs/NEPCMs are shown in Figs. 6.15(a-f). The TES system is charged with the help of water as HTF, which circulated from the HTF tank through a magnetic drive pump to a shell-and-tube-type heat exchanger at a constant flow rate of 2 LPM, which was measured with the rotameter as discussed in the earlier chapter.

Fig.6.14(a). Front view of the Experimental setup

Fig.6.14(b). Side view of the Experimental setup

The thermocouples with a datalogger were used for measuring the temperature and the temperature readings were taken at a regular interval of 5sec throughout the charging period for various NEPCMs. The experiment was performed on a 7kg engine load with 1500 RPM.

Fig 6.15(a). Inline tubes arrangement

Fig 6.15(b). Staggered tubes arrangement

Fig.6.16(a). LA+0.1% Al_2O_3 (liquid state)

Fig.6.16(b). PW+0.02% MWCNT (liquid state)

Fig.6.16(c). SA+0.1% CuO (liquid state)

Fig.6.16(d). LA+0.1% Al_2O_3 (solid state)

Fig.6.16(e). PW+0.02% MWCNT (solid state)

Fig.6.16(f). SA+0.1% CuO (solid state)

Table 6.2: Specification of tubes used in TES systems

Specification	Inner Tube	Outer Tube
Tube diameter	1.27cm	2.54cm
Wall thickness	0.125cm	0.165cm
Material	Stainless steel (304) (Cr-18%,Ni-8%,C-0.08%)	Stainless steel (304) (Cr-18%,Ni-8%,C-0.08%)
Thermal conductivity	14 W/m.K	14 W/m.K
Specific heat	490 J/kg.K	490 J/kg.K
Melting point	1673 K	1673 K
Number of tubes	5	5

6.2.2. Data Reduction

The charging profile and the energy storage of NEPCM/PCM filled inline and staggered tube bundles type TES system have been calculated. Furthermore, results in the discussion have been done on the inline and staggered tube bundles type TES system integrated with IC engine during air heating. Also, the variation in heat transfer rate from the TES system to ambient air has been examined.

6.2.2.1. Charging profile of NEPCM/PCM filled inline and staggered tube bundles type TES system

Figs. 6.17(a-d) shows the charging profile of the TES system, which was filled with 0.1% vol. fraction of Al_2O_3-based lauric acid NEPCM/PCM. Results revealed that in the case of Al_2O_3 based lauric acid NEPCM filled in staggered tube bundles, the TES system required 37.5%, 14.33%, and 7% less charging time than lauric acid in inline, staggered, and lauric acid with Al_2O_3 nanoparticles for inline tube bundles type based TES systems, respectively.

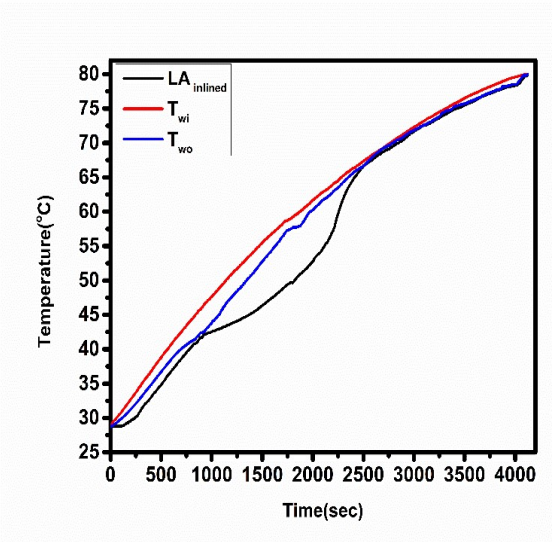

Fig.6.17(a). Lauric acid filled in inline TES system

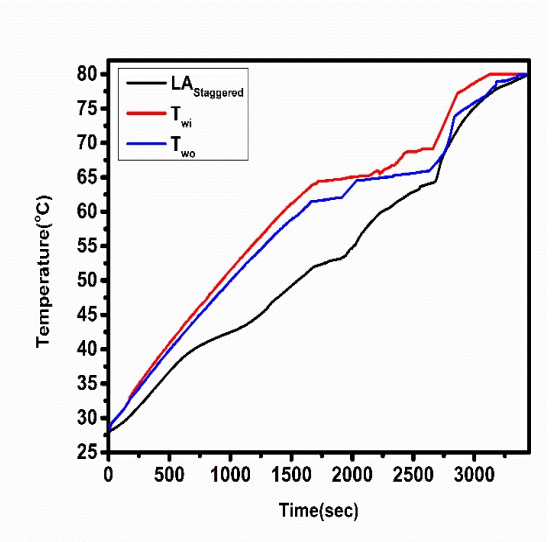

Fig.6.17(b). Lauric acid filled in staggered TES system

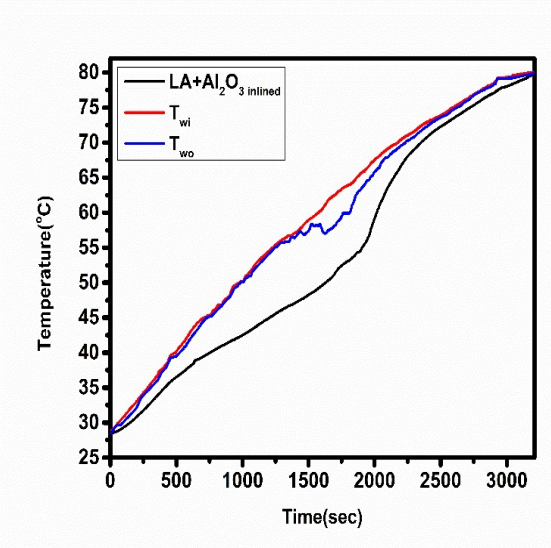

Fig.6.17(c). Lauric acid with Al_2O_3 filled in inline TES system

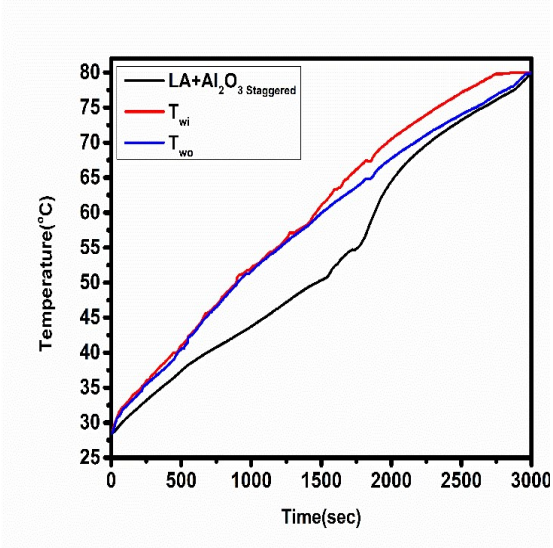

Fig.6.17(d). Lauric acid with Al_2O_3 filled in staggered TES system

In the next case, 0.02% vol. fraction of MWCNT-based paraffin wax NEPCM/PCM was filled in the TES system as shown in Figs. 6.18(a-d). It is observed that in the case of MWCNT based PW NEPCM filled in staggered tube bundles, the TES required 28%, 11%, and 4.26% less charging time than paraffin wax. in inline, staggered, and paraffin wax with MWCNT nanoparticles inline tube bundles type TES systems, respectively.

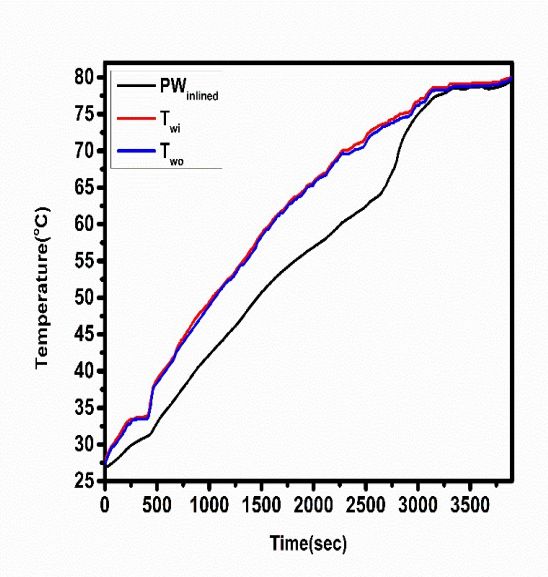

Fig.6.18(a). Paraffin wax filled in inline TES system

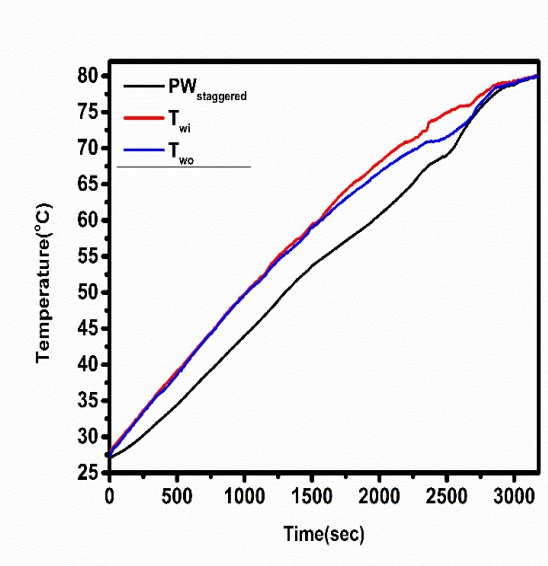

Fig.6.18(b). Paraffin wax filled in staggered TES system

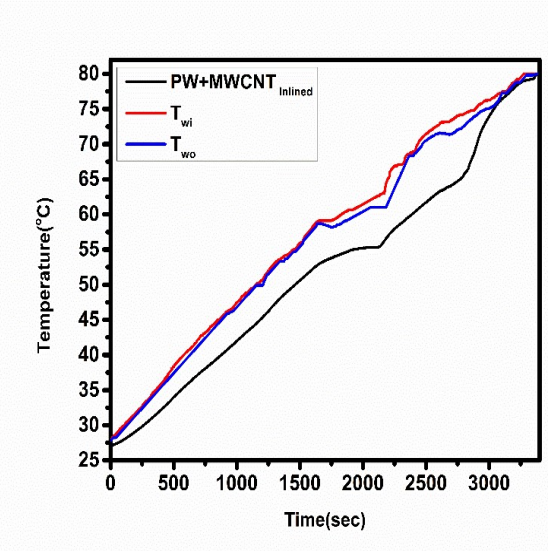

Fig.6.18(c). Paraffin wax with MWCNTfilled in inline TES system

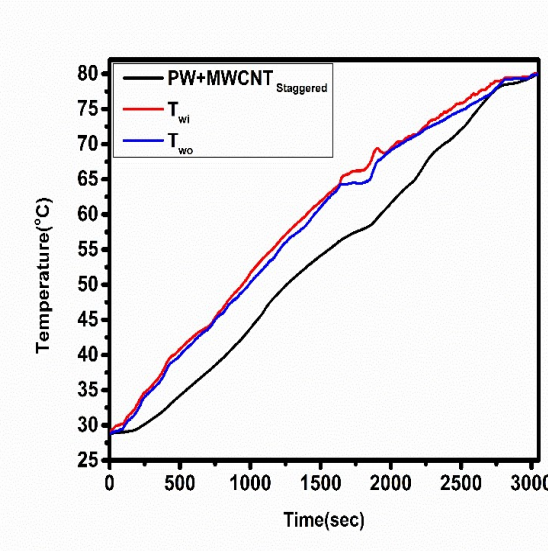

Fig.6.18(d). Paraffin wax with MWCNT filled in staggered TES system

However, Figs. 6.19(a-d) shows the charging temperature profile of 0.1% vol. fraction of CuO-based stearic acid NEPCM/PCM filled in the TES system. In the case of CuO-based stearic acid NEPCM filled in staggered tube bundles, the TES system required 47%, 31%, and 10.3% less charging time than stearic acid in inline, staggered, and stearic

acid. With CuO nanoparticles inline tube bundles type based TES systems, respectively. It is also observed that the maximum heat transfer occurs at the phase change state.

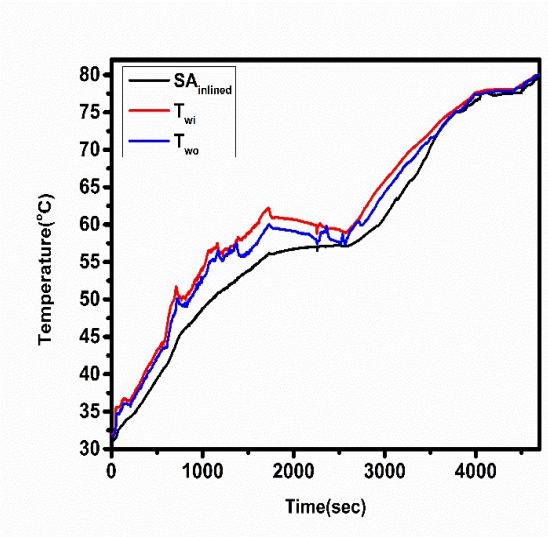

Fig.6.19(a). Stearic acid filled in inline TES system

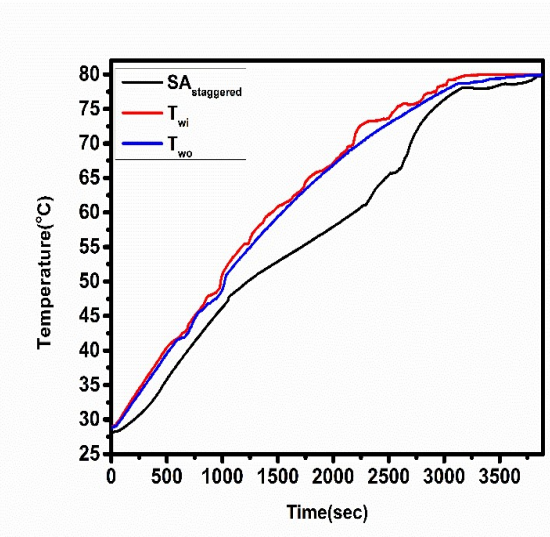

Fig.6.19(b). Stearic acid filled in staggered TES system

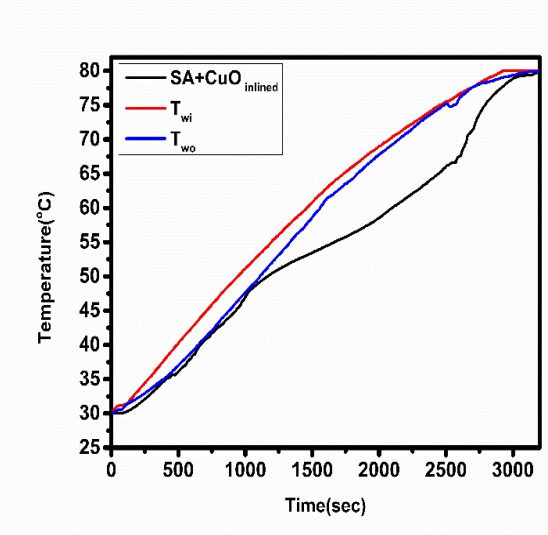

Fig.6.19(c). Stearic acid with Al_2O_3 filled in inline TES system

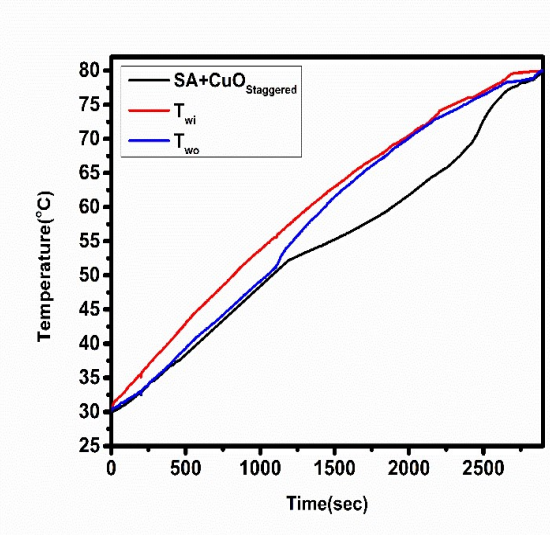

Fig.6.19(d). Stearic acid with Al_2O_3 filled in staggered TES system

6.2.2.2. Energy storage of NEPCM/PCM filled inline and staggered tube bundles type TES system

The energy stored in the TES system is filled with 0.1% vol. fraction of Al_2O_3-based lauric acid, 0.02% vol. fraction of MWCNT-based paraffin wax and 0.1% vol. fraction of CuO-based stearic acid PCM/NEPCMs, respectively, were shown in Figs. 6.20(a-c). It has been observed that 0.1% vol. fraction of Al_2O_3 in lauric acid-based staggered tube arrangement TES system, the maximum energy storage was 21.6%, 14.68%, and 8.16% higher than lauric acid in inline, staggered, and lauric acid with 0.1% vol. fraction of Al_2O_3 nanoparticles inline tube bundles type TES systems, respectively. However, the maximum energy storage in the case of 0.02% vol. fraction of MWCNT in paraffin wax during staggered tube arrangement TES system was 14.6%, 10.3%, and 4.88% higher than paraffin wax in inline, staggered, and paraffin wax MWCNT nanoparticles for inline tube bundles type TES systems, respectively.

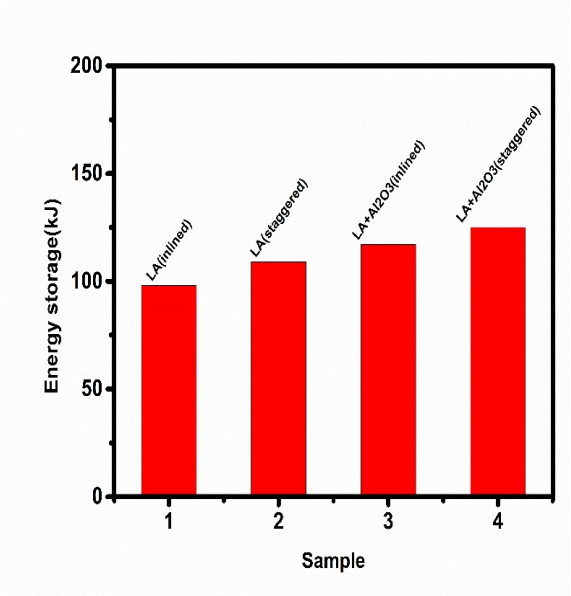

Fig.6.20(a). Lauric acid PCM/NEPCM based TES system

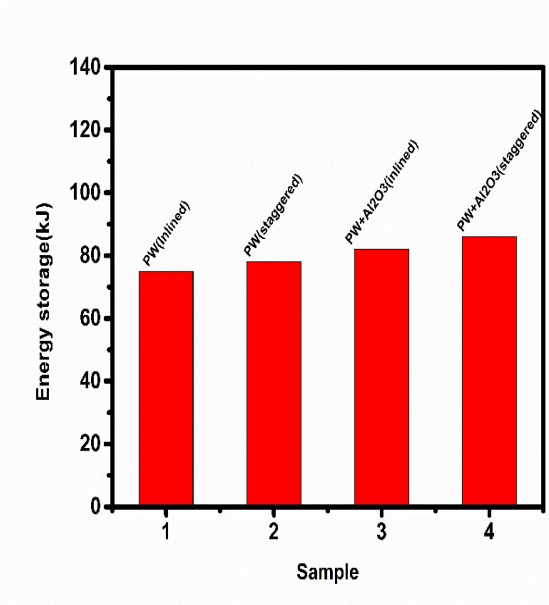

Fig.6.20(b). Paraffin wax PCM/NEPCM based TES system

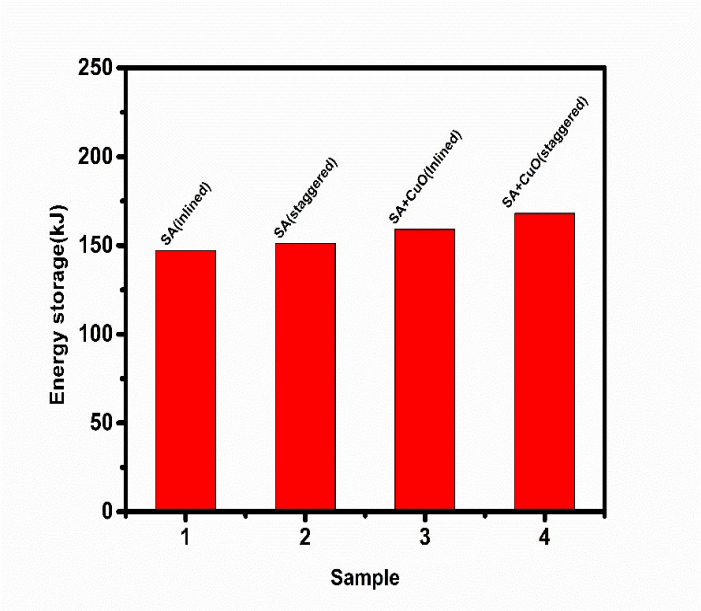

Fig.6.20(c). Stearic acid PCM/NEPCM based TES system

Furthermore, the maximum energy storage in the case of 0.1% vol. fraction of CuO-based stearic acid NEPCM during staggered tube arrangement TES system was 14.28%,11.25%, and 5.66% higher than SA in inline, staggered, and SA with CuO nanoparticles for inline tube bundles type TES systems, respectively.

6.2.2.3. Inline and staggered tube bundles type TES system integrated with IC engine for air heating

The profile of air outlet temperature was shown in Figs. 6.22(a-d), and Figs. 6.23(a-d) when the air flowed over the charged TES system filled with 0.1% vol. fraction of Al_2O_3-based lauric acid, 0.02% vol. fraction of MWCNT-based paraffin wax and 0.1% vol. fraction of CuO-based stearic acid PCM/NEPCMs, respectively. The maximum temperature difference between the outlet and inlet air was 8.6°C for 0.1% vol. fraction of Al_2O_3 in lauric acid-based staggered tube arrangement TES system. Also, the TES system was 48.2%, 34.88%, and 25.6% higher than the lauric acid inline and staggered and 0.1% vol. fraction of Al_2O_3-based lauric acid inline tube arrangement TES systems

as shown in Figs. 6.21(a-d). In a different case, the maximum temperature difference between outlet and inlet air was 8.4°C found in 0.02% vol. fraction of MWCNT-based paraffin wax staggered tube arrangement TES system. However, this system has 15.47%, 7.1%, and 5.1% higher temperature differences than paraffin wax inline and staggered and 0.02% vol. fraction of MWCNT-based paraffin wax inline tube arrangement TES systems as shown in Figs. 6.22(a-d). Also, the maximum temperature difference between outlet and inlet air was 7.7°C in 0.1% vol. fraction of CuO in stearic acid staggered tube arrangement TES system. It has a 28.6%, 9%, and 4% higher temperature difference than stearic acid for inline and staggered and 0.1% vol. fraction of CuO in stearic acid inline tube arrangement TES system as shown in Figs. 6.23(a-d).

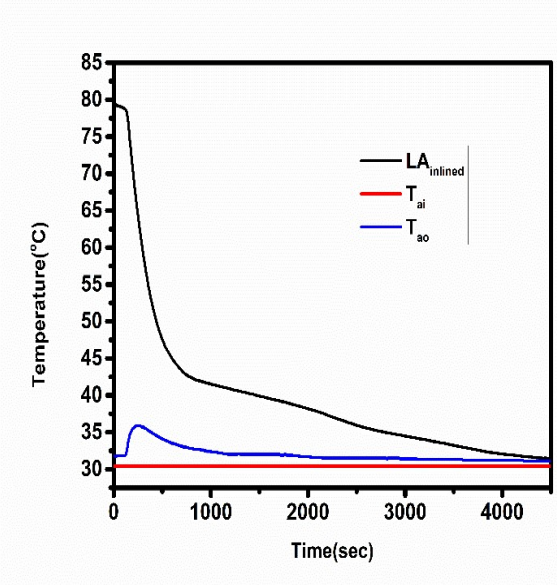

Fig.6.21(a). Lauric acid filled in inline TES system

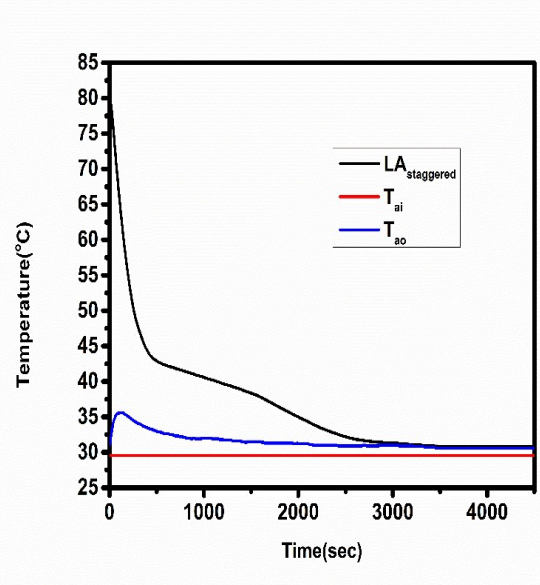

Fig.6.21(b). Lauric acid filled in staggered TES system

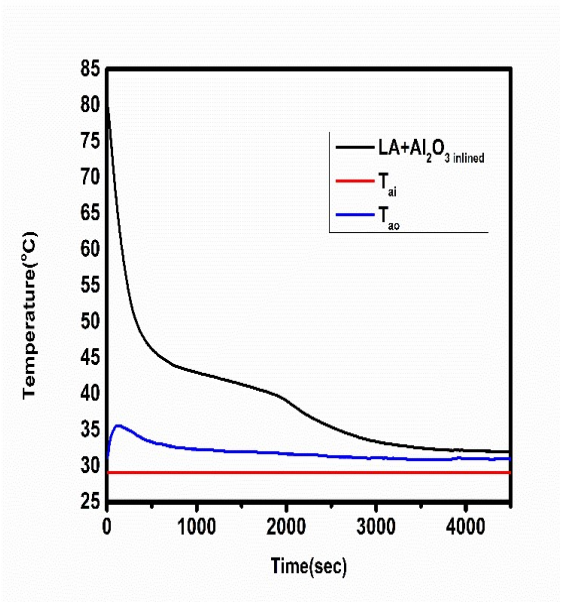

Fig.6.21(c). Lauric acid with Al_2O_3 filled in inline TES system

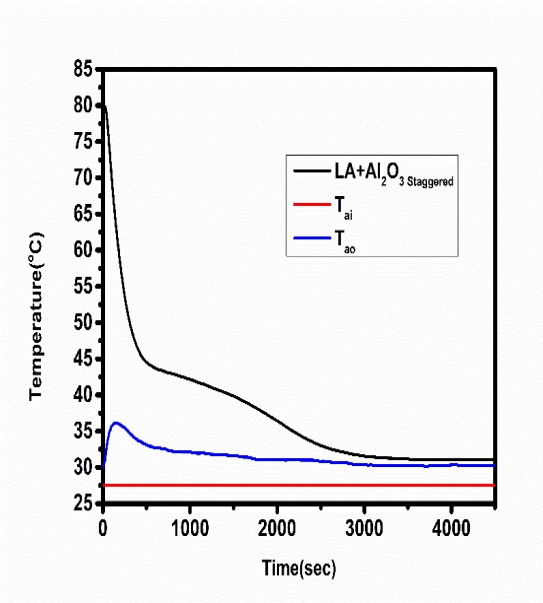

Fig.6.21(d). Lauric acid with Al_2O_3 filled in staggered TES system

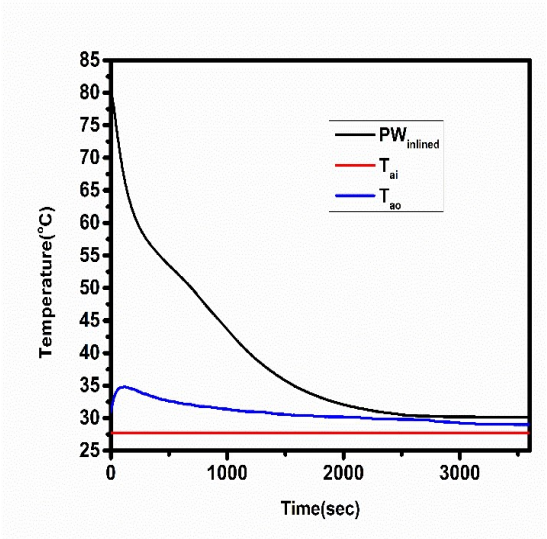

Fig.6.22(a). Paraffin wax filled in inline TES system

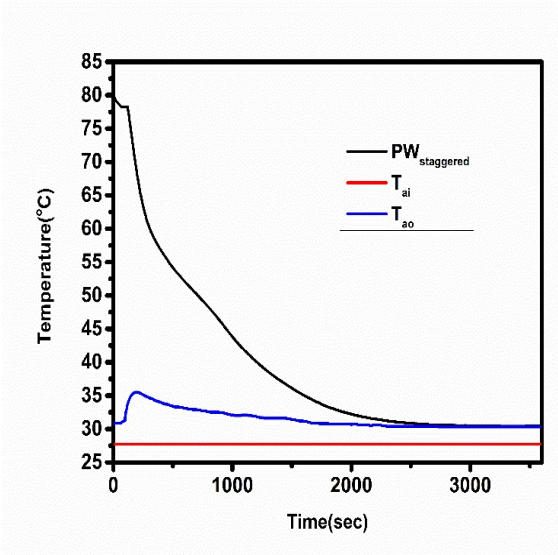

Fig.6.22(b). Paraffin wax filled in staggered TES system

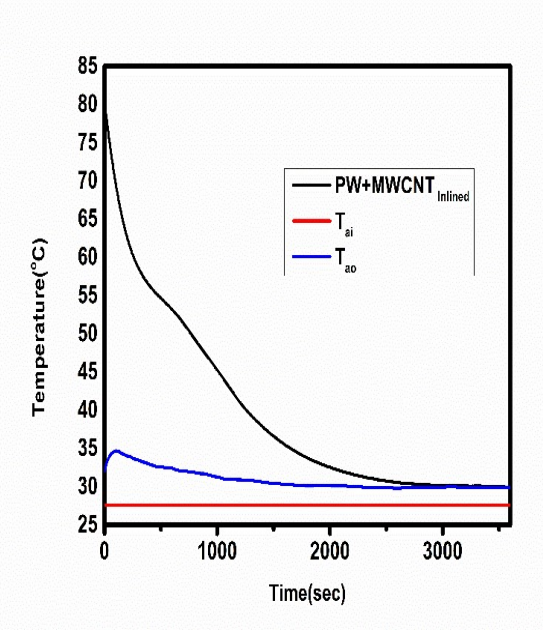

Fig.6.22(c). Paraffin wax with MWCNTfilled in inline TES system

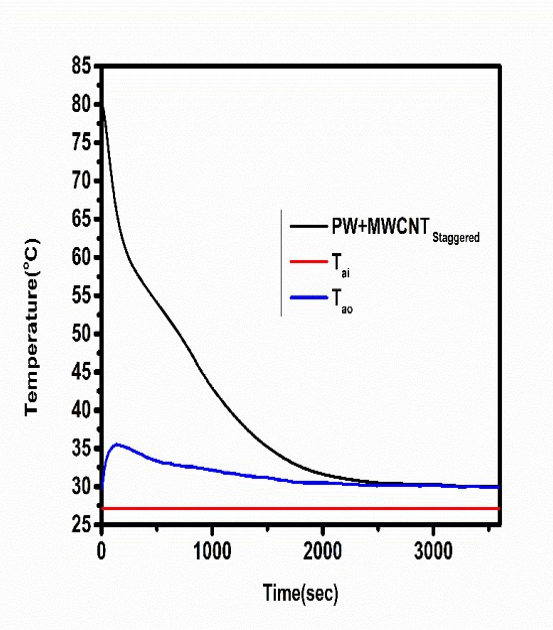

Fig.6.22(d). Paraffin wax with MWCNTfilled in staggered TES system

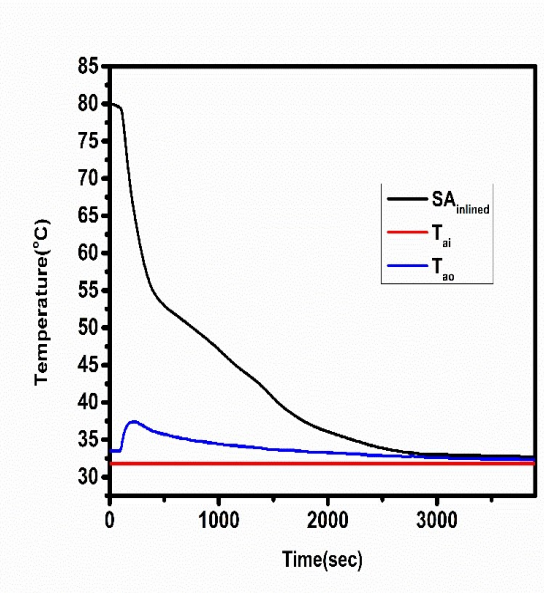

Fig.6.23(a). Stearic acid filled in inline TES system

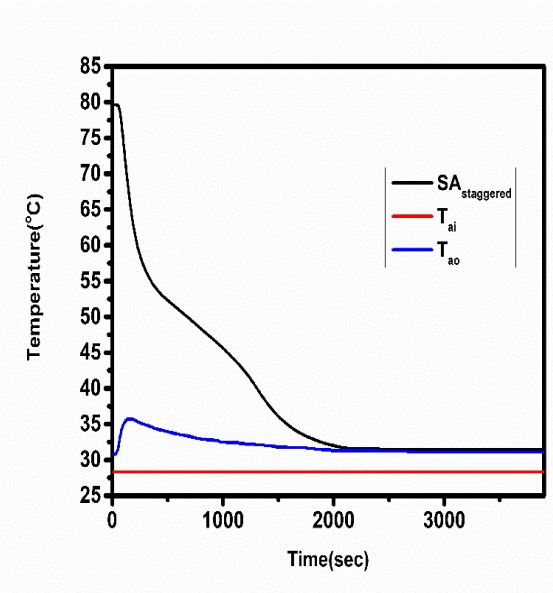

Fig.6.23(b). Stearic acid filled in staggered TES system

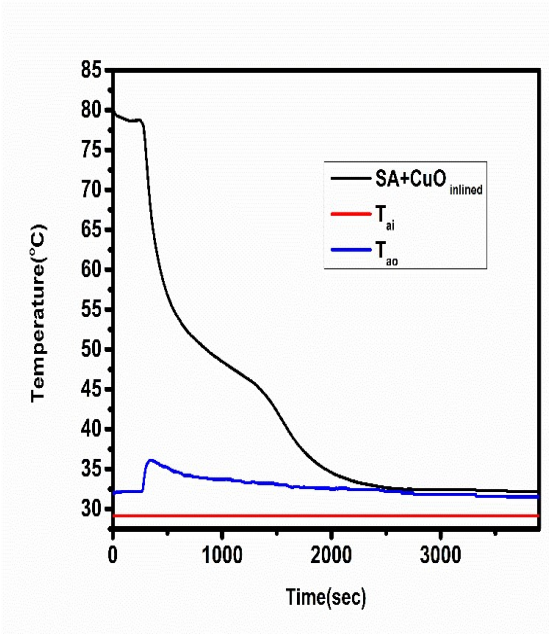

Fig.6.23(c). Stearic acid with Al_2O_3 filled in inline TES system

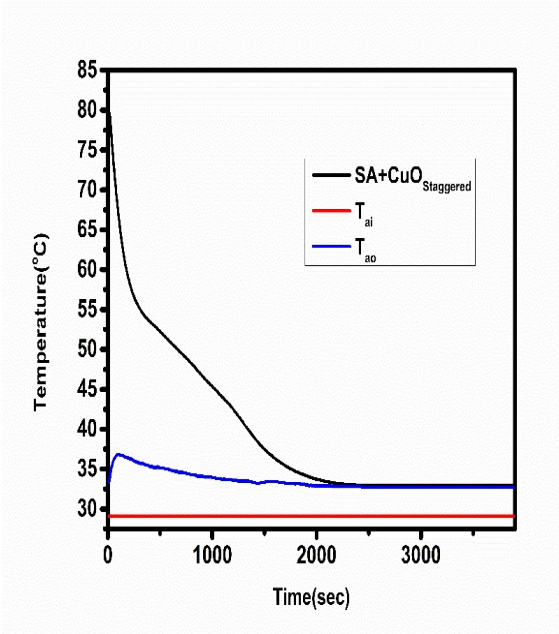

Fig.6.23(d). Stearic acid with Al_2O_3 filled in staggered TES system

6.2.2.4.The variation in heat transfer rate

The variation in heat transfer rate from the TES system to ambient air has been examined. The inline and staggered tubes arrangement-type TES systems have been used for experimenting. The TES system was filled with 0.1% vol. fraction of Al_2O_3-based lauric acid, 0.02% vol. fraction of MWCNT-based paraffin wax and 0.1% vol. fraction of CuO-based stearic acid PCM/NEPCMs, respectively. Results revealed that the heat transfer rate for 0.1% vol. the fraction of Al_2O_3-based lauric acid-based staggered tube arrangement TES system was 52.72% and 40% higher than lauric acid-based inline and staggered tube arrangement type TES systems. Also, it results in a 35.4% higher heat transfer rate than 0.1% vol. fraction of Al_2O_3 in lauric acid-based inline tube arrangement TES system as shown in Fig.6.24(a). However, the heat transfer rate of 0.02% vol. The fraction of MWCNT in the paraffin wax-based staggered tube arrangement TES system was 19.11% and 20.14% higher than in paraffin wax-based inline and staggered tube

arrangement type TES systems. In addition, as shown in Fig. 6.24(b), the heat transfer rate was 5.2% greater than the 0.02% vol. fraction of MWCNT in paraffin wax-based inline tube arrangement TES system. Results also revealed that the heat transfer rate of 0.1% vol. fraction of CuO in stearic acid-based staggered tube arrangement TES system was 44.4% and 14.7% higher than stearic acid-based inline and staggered tube arrangement type TES systems, respectively, as shown in Fig. 6.24(c). Furthermore, the heat transfer rate was 2.63% higher than 0.1% vol. fraction of CuO in stearic acid-based inline tube arrangement TES system.

Lastly, the heat transfer rate from the TES system to the ambient air revealed an optimum result in the case of 0.1% vol. fraction of Al_2O_3 in lauric acid-based staggered tube arrangement TES system compared to MWCNT in paraffin wax and CuO in stearic acid PCM based TES systems.

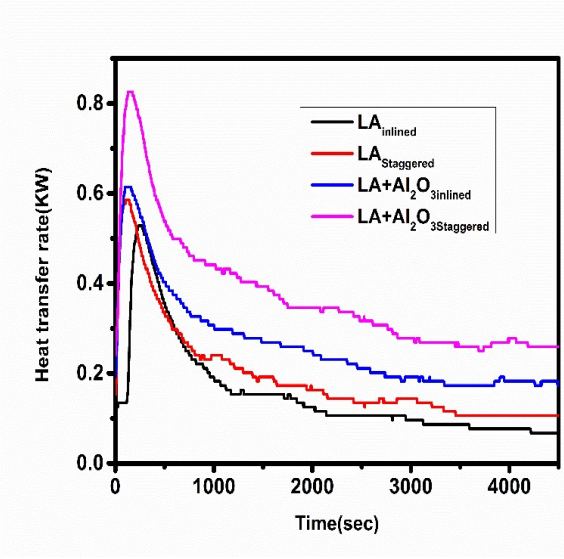

Fig.6.24(a). Lauric acid PCM/NEPCM based TES system

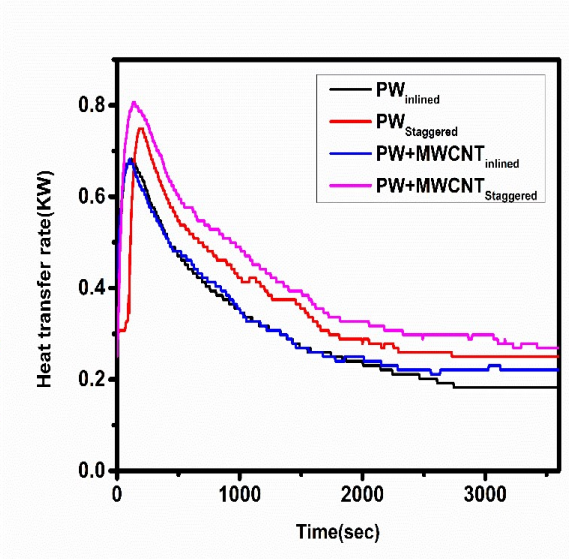

Fig.6.24(b). Paraffin wax PCM/NEPCM based TES system

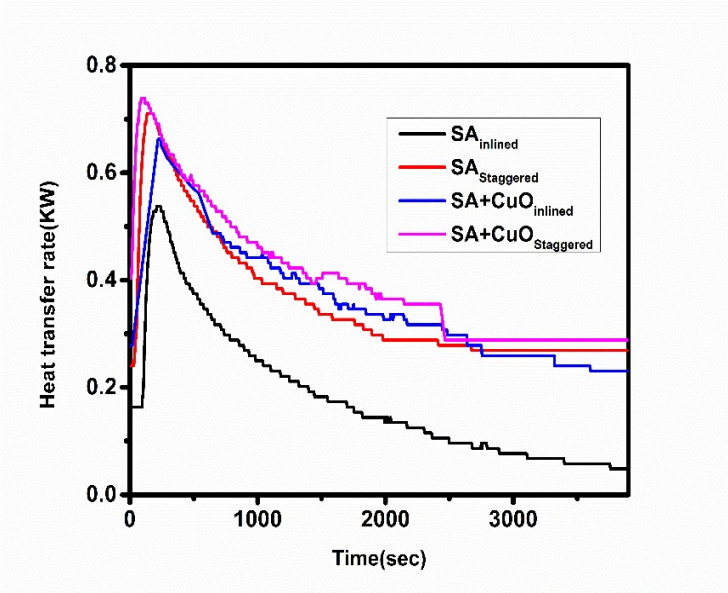

Fig.6.24(c). Stearic acid PCM/NEPCM based TES system

6.3. Application of the waste heat recovery for cabin heating

A cabin with a volume capacity of $1m^3$ has been heated by using the waste heat recovered from an IC engine's exhaust. The cabin was fabricated with wooden pieces and well insulated with extruded polystyrene (XPS). Fig. 6.25 shows the cabin attachment with the experimental apparatus. A staggered tube arrangement TES system loaded with 0.1% vol to fraction of Al_2O_3-based lauric acid to explore the best outcomes. The cabin temperature was reduced with an increment in air velocity from 2 to 4m/s. At air velocities of 2m/s, 3m/s, and 4m/s, the maximum temperature of the cabin was 6.2°C, 5.5°C, and 4.3°C higher than the ambient temperature, as shown in Figs. 6.26(a-c).

Fig.6.25. Experiment apparatus with cabin attachment

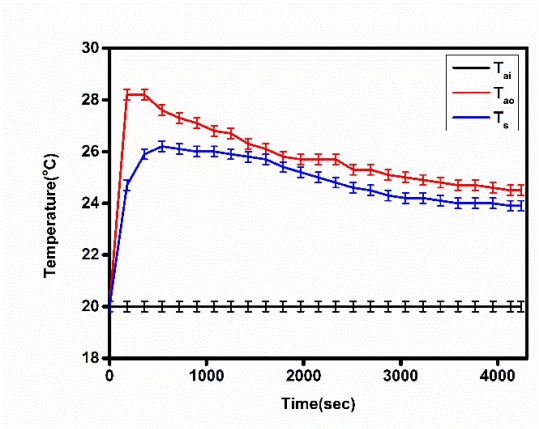

Fig.6.26(a). Variation in-cabin temperature at air velocity 2m/s

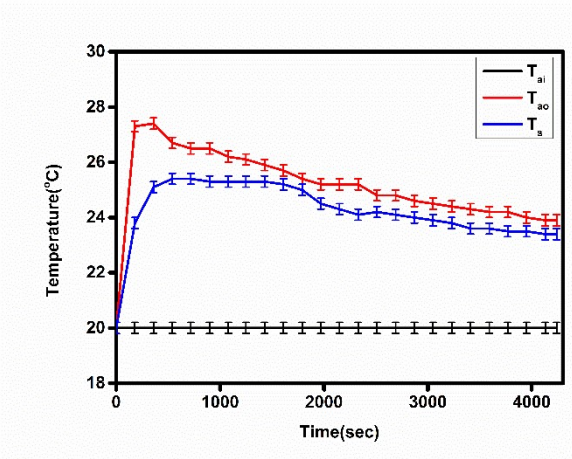

Fig.6.26(b). Variation in-cabin temperature at air velocity 3m/s

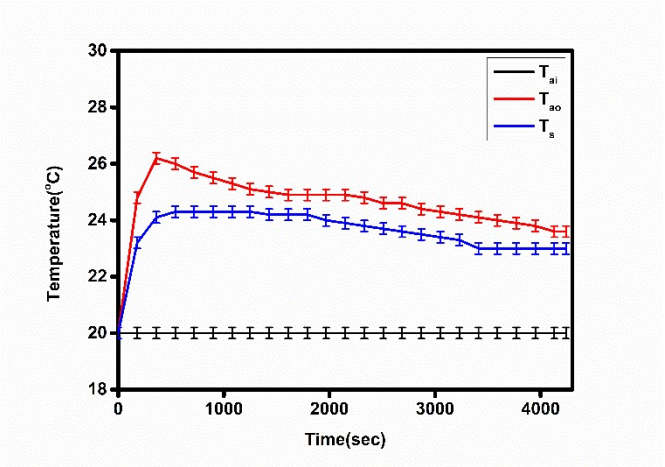

Fig.6.26(c). Variation in-cabin temperature at air velocity 4m/s

This chapter has comparative studies for inline and staggered tube bundles type-based TES systems with various geometric parameters. The staggered tube bundles type TES system shows an optimum thermal performance compared to other considered TES systems. On the basis of experimental studies, the lauric acid with 0.1% vol. fraction Al_2O_3-based NEPCM filled in staggered tube bundles type TES system has a maximum air temperature variation than other NEPCMs. Also, the lauric acid with 0.1% vol. fraction Al_2O_3-based NEPCM filled in staggered tube bundles type TES system achieved 6.2°C higher temperature in a cabin at an air velocity of 2m/sec. Furthermore, the variation in error value for cabin temperature was obtained to be 0.2-0.6°C.

6.4. Economic analysis of PCMs/NEPCMs based on TES system

An economic analysis is conducted to determine the system's monetary feasibility. The overall cost of the structure is the sum of the individual material costs and the fabrication costs in each case.

$$S\,(Rs) = S_{TES} + S_{PCM} + S_{NP/MWCNT} + S_{pump} + S_{HEX} + S_{tank} + S_{Air\ blower} + S_{Fabrication} \qquad 6.7(a)$$

Where, S represents the overall cost of the fixed structure.

Similarly, S_{TES}, S_{PCM}, $S_{NP/MWCNT}$, S_{pump}, S_{HEX}, S_{tank}, $S_{Air\ blower}$, and $S_{Fabrication}$ represent the Cost of the TES, PCM, nanoparticles/multiwall carbon nanotubes, magnetic pump, heat exchange, tank, air blower, and fabrication respectively.

$$R\ (Rs) = R_{air\ blower} + R_{Pump} \qquad 6.7(b)$$

Where R represents the total running cost for one year when air blower and pump are operated for 8 hours per day.

Similarly, $R_{air\ blower}$= Running cost of air blower

R_{Pump} = Running cost of magnetic pump

The cost of energy produced by the system should be estimated to determine the overall cost savings from using it. Energy recovered by the system is utilized for heating cabin space, having a capacity of $1m^3$.

$$Q_{cabin}\ (kW) = \dot{m} \times C_{p\ air} \times \Delta T \qquad 6.7(c)$$

Where, Q_{cabin} represents the heat required for cabin space heating. $\dot{m}$ and ΔT denotes air mass flow rate and increment in cabin space temperature, respectively.

However, using a typical electric water heater to heat the cabin space seems to be efficient. Assuming a 75% electric efficiency, the heater's annual electricity usage (E) is calculated as follows:

$$E\ (kW) = \frac{Q_{cabin}}{0.75} \qquad 6.7(d)$$

The quantity of power used for cabin space heating is saved if the TES system is operational for 8 hours per day throughout the year. The total running cost for the electric heater:

$$R_{Electricity\ heater}(Rs) = E \times duration \times No.\ of\ days \times Cost\ of\ electricity\ per\ unit \quad 6.7(e)$$

Total running cost of saving per year, $R_{Total}(Rs) = R_{Electricity\ heater} - R$ 6.7(f)

However, the payback duration is the amount of time it takes to repay an investment's cost or reach the breakeven point for an investor. Longer payback periods are less desired, whereas shorter payback periods are more desirable. The payback duration (PBD) is estimated as follows:

$$PBD = \frac{\text{The overall cost of the structure}}{\text{Total running cost of saving per year}} \quad 6.7(g)$$

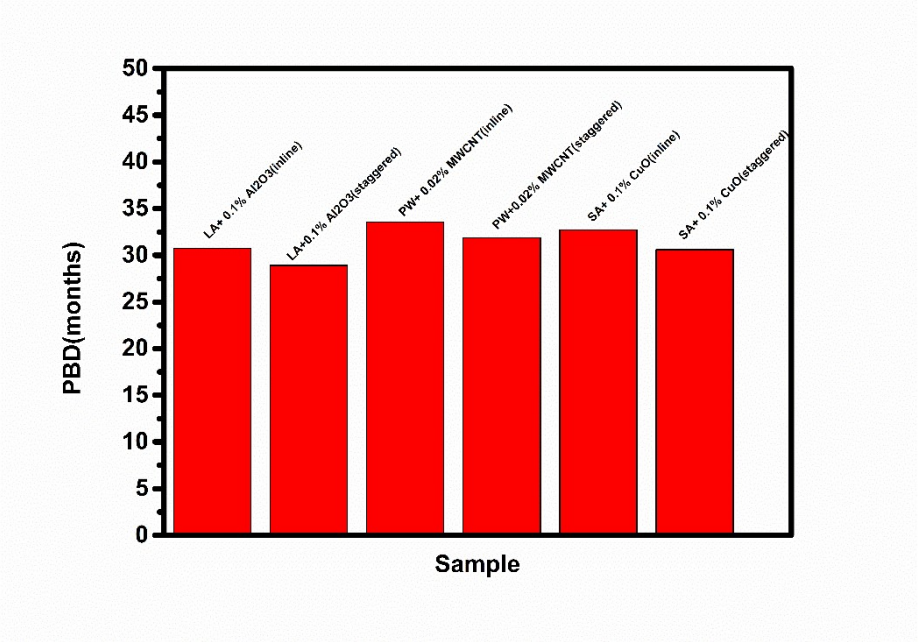

Fig.27. Payback duration of PCMs/NEPCMs based TES system

Fig.27 shows the variation of payback durations of PCMs/NEPCMs based on a TES system integrated with an IC engine for cabin space heating with a 1 m^3 volume capacity. Results revealed that due to increment in temperature of cabin space in case of staggered tube arrangement than inline tube arrangement, the payback duration is higher. In a staggered tubes arrangement type TES system, the payback period of LA with 0.1%

vol. fraction of Al_2O_3-based TES system is 10.24% and 5.84% less than PW with 0.02% vol. fraction of MWCNT and SA with 0.1% vol. fraction of CuO, respectively.

6.5. Highlights

- The present comparative studies revealed that staggered tube bundles type TES system shows an optimum thermal performance compared to other considered TES systems.
- Results revealed that 0.1% vol. fraction of Al_2O_3 in based lauric acid NEPCM filled in staggered tube bundles type TES system was 37.5%, 14.33%, and 7% less charging time than lauric acid in inline, staggered, and Al_2O_3 in lauric acid-based inline tube bundles type TES systems, respectively.
- Also, results revealed that 0.02% vol. fraction of MWCNT in paraffin wax filled in staggered tube arrangement TES system was 28%, 11%, and 4.26% less charging time than paraffin wax in inline, staggered, and paraffin wax with MWCNT inline tube arrangement TES systems, respectively.
- The experimental study revealed that maximum energy storage for 0.02% vol. fraction of MWCNT in paraffin wax-based staggered tube arrangement TES system was 14.6%, 10.3%, and 4.88% higher than paraffin wax in inline, staggered, and paraffin wax with MWCNT inline tube bundles type TES systems, respectively.
- Also, the maximum energy storage for stearic acid with 0.1% vol. fraction based NEPCM filled in staggered tube bundles type TES system was 14.28%,11.25%, and 5.66% higher than SA in inline, staggered, and SA with CuO nanoparticles inline tube bundles type TES system, respectively.

- An experimental study revealed that the lauric acid with 0.1% vol. fraction Al_2O_3-based NEPCM filled in staggered tube bundles type TES system has a maximum air temperature variation than other NEPCMs.
- Furthermore, the lauric acid with 0.1% vol. fraction Al_2O_3-based NEPCM filled in staggered tube bundles type TES system achieved 6.2^oC higher temperature in a cabin at an air velocity of 2m/sec.

This page is intentionally left blank